Utilizing redox-chemistry to elucidate the nature of exciton transitions in supramolecular dye nanotubes

Eisele, D. M.; Cone, C. W.; Bloemsma, E. A.; Vlaming, S. M.; van der Kwaak, C. G. F.; Silbey, R. J.; Bawendi, M. G.; Knoester, J.; Rabe, J. P.; Vanden Bout, D. A.

Published in:
Nature Chemistry

DOI:
10.1038/NCHEM.1380

nature chemistry

SUPPLEMENTARY INFORMATION

DOI: 10.1038/NCHEM.1380

Utilizing Redox-Chemistry to Elucidate the Nature of Exciton Transitions in Supramolecular Dye Nanotubes

D. M. Eisele[1,2], C. W. Cone[3], E. A. Bloemsma[4],
S. M. Vlaming[1,4], C.G.F. van der Kwaak[4], R. J. Silbey[1,†], M. G. Bawendi[1],
J. Knoester[4,*], J. P. Rabe[2], and D. A. Vanden Bout[3,*]

[1] Massachusetts Institute of Technology,
Center for Excitonics and
Department of Chemistry, Cambridge, *USA;*

[2] Humboldt-Universität zu Berlin,
Department of Physics and IRIS Adlershof, Berlin, *Germany;*

[3] University of Texas at Austin,
Department of Biochemistry and Chemistry and
Center for Nano and Molecular Science and Technology, Austin, *USA*;

[4] University of Groningen,
Institute for Theoretical Physics and
Zernike Institute for Advanced Materials, Groningen, *The Netherlands*;

[†]*Author deceased*

* Corresponding authors:
j.knoester@rug.nl (theory) and
dvandenbout@mail.cm.utexas.edu (experiment)

Table of Contents:

1. No changes of nanotube's double-walled morphology upon oxidation

Line scans of the CryoTEM data (**Figure S1**) taken across the nanotubes before and after oxidation (red solid line and green solid line, respectively) reveal that first, the double-walled morphology of the nanotubes is maintained and second, the diameter of the two nanotubes is unchanged by the oxidation.

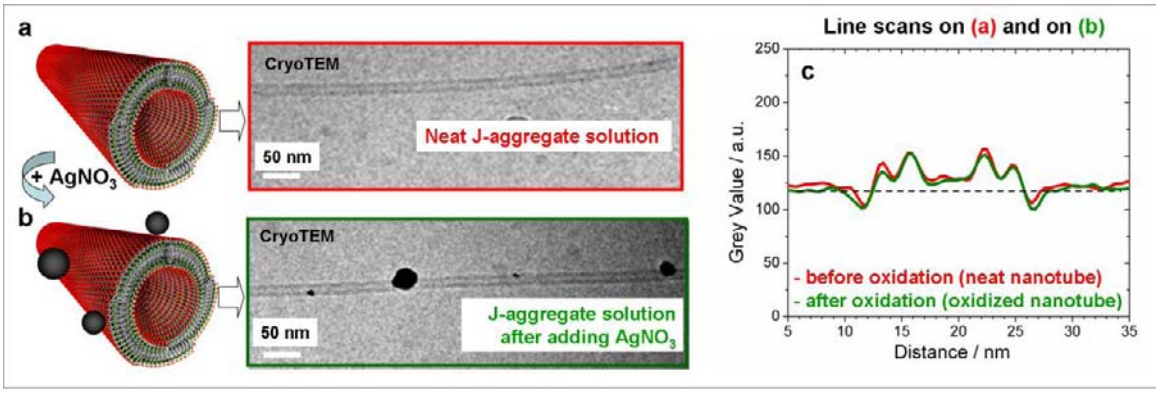

Figure S1: Representative Cryo-TEM micrographs of the **(a)** neat nanotubular dye aggregate solution without $AgNO_3$ (red box) and **(b)** with $AgNO_3$ (green box). Line scans reveal no significant changes of the nanotube's double-walled morphology upon oxidation by $AgNO_3$. **(c)** Line scans taken on (a) (red) and on (b) (green); the two traces across the nanotubes are not significantly different indicating that the double-walled character of the nanotube is maintained and the diameters of the inner and outer wall cylinders are not significantly altered upon oxidation (see also [1]).

2. Singular Value Decomposition (SVD)

The Singular Value Decomposition (SVD) is a method based on linear algebra that analyzes the changes in a data set (containing *n* data) and describes this data set as a linear combination of *n* basis functions. The SVD results in multiplets of basis functions that are sorted by their singular value (SV), which gives the importance of each basis function: the basis functions with the *m* non-zero SVs provide the best least squares approximation to the data that can be determined with these m basis functions, with $m<n$ [2]. Thus, the number of components *m* will be given by the number *m* of non-zero SVs, so it should be exactly *m* components for *m* expected spectral features. The data set of the 10 spectra depicted in **Figure 2c** was analyzed by SVD.

The results of the analysis are presented in **Figure S2**, which shows the SVs plotted over the number of the basis function *n*, with *n*=1, 2,...,9 ,10. Most interestingly, only two SVs that are significantly different from zero are obtained.

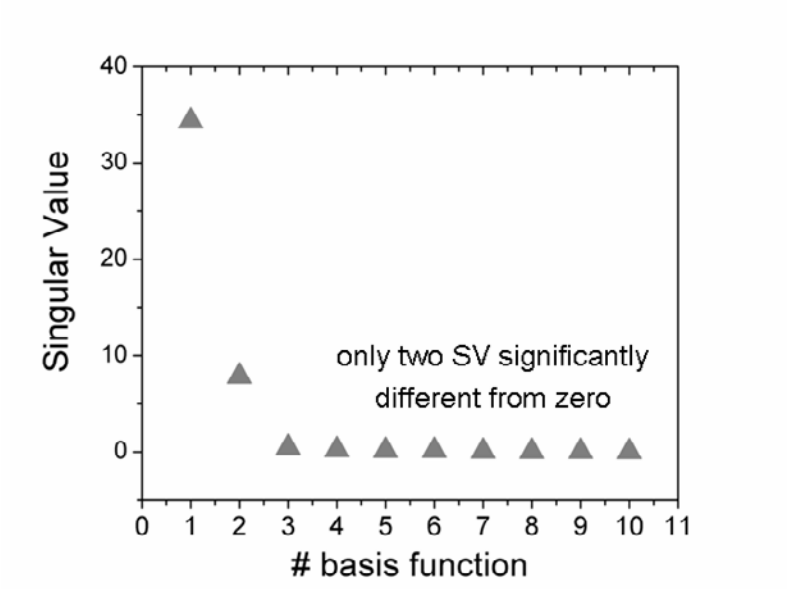

Figure S2: Singular Values (SV) of data set shown in (a) analyzed by Singular Value Decomposition. Only two SV are significantly different from zero. The SVs of these two basis spectra demonstrate that they account for over 99.97% of the variance in the entire data set shown in **Figure 2c**.

3. Spectral changes of dye aggregate solution upon chemical oxidation

Analysis of the spectral changes in **Figure 2c** reveals that near the end of the reaction the contribution from one species has been completely eliminated, as further oxidation leads to a decrease in absorption amplitude but not to a change in spectral shape. In other words, it can be assumed that the outer wall cylinder is completely oxidized and can no longer contribute to the light-harvesting nanotubes' optical response. As the redox reaction goes on, the dye molecules in the inner wall cylinder are oxidized as well. In case the inner wall cylinder can be seen as a separate system, the oxidation of the inner wall dye molecules consequently leads to a loss in overall intensity. On the other hand, changes in the absorption spectrum's shape are expected when further oxidation modifies the nature of the intermolecular excitonic coupling within the inner wall cylinder.

As shown in **Figure S3**, the last three spectra are identical except for the overall amplitude. Consequently, this final spectrum (green line) can be assigned to the residual absorption of a single cylindrical dye aggregate (in the presence of the other, completely oxidized cylindrical dye aggregate).

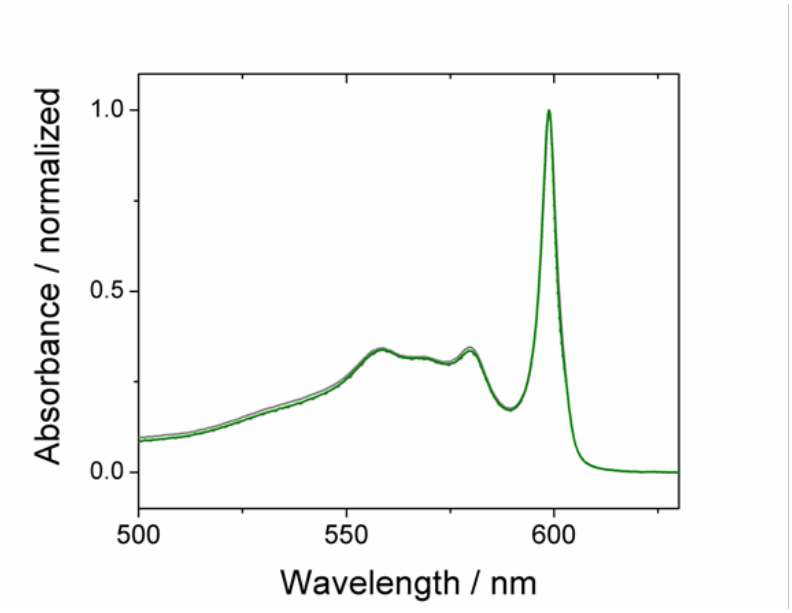

Figure S3: Final three absorption spectra shown in **Figure 2c**, normalized to have the same absorbance value at a wavelength of 599 nm.

4. Novel Extended Herringbone-like (EHB) Structure and Exciton Hamiltonian

The route towards the Extended Herringbone-like structure:

Structural models for single cylindrical aggregates can be obtained by wrapping two-dimensional sheets of molecules around a cylindrical structure. To design a new valid geometrical model for the double-walled nanotubes, we first simulated the optical response of a single cylinder and compared the simulations with the experimental data obtained from the isolated inner wall cylinder of the double-walled light-harvesting nanotube (**Figure 3b**). The validity of the structural model requires that it correctly reproduces the (relative) energies, polarization directions, and intensities of the four absorption bands observed in the experimental inner wall spectrum. The thus obtained model for the inner wall cylinder was also used as the geometrical model for the outer wall cylinder. Comparison of the simulations for the full double-walled nanotubes with the experimental spectrum then determines the specific details of the molecular arrangements within the outer wall cylinder. Here we presumed that the coupling between both cylindrical walls is weak enough to neglect the occurrence of coherent exciton states shared by both.

As a starting point for the geometry of a single aggregate, we used a regular planar lattice of unit cells, where each unit cell consists of two C8S3 molecules. The two molecules per unit cell configuration is necessary to explain the total number of four absorption bands seen in the experimental inner wall spectrum. In contrast, a model with one molecule per unit cell generally yields only two absorption bands [3]. We have simulated several classes of structural models where the molecules (bricks) *remain in the plane* that is rolled onto a cylindrical surface of the appropriate circumference. These classes of structures contained several variations on both bricklayer structures and Herringbone structures.

Common to all these structural models is that the simulation of their linear optical response (not shown here) leads to intensities of the high-energy transitions, i.e. transitions (4) and (5) in **Figure 3b**, which are significantly too small in comparison with the experimental data. Interestingly, of these structures only the Herringbone model could correctly reproduce the energy positions and the polarizations of the four transition bands in the experimental absorption spectrum of the isolated inner wall cylinder. The polarizations of the four inner wall transitions were assigned based on previous linear dichroism experiments [4]. To increase the strength of the high-energy transitions (4) and (5), we used a Herringbone structure but, in addition, allowed the molecules to be *tilted out of the plane*. This is the new Extended Herringbone-like (EHB) structure (detailed description in text below). We also tested several variations of the EHB structure, but these structures typically necessitate additional fit parameters, which makes it very difficult to search the entire parameter space in order to find the optimal fit. Moreover, these geometries also did not give significantly better agreement with the experimental data than the fits obtained using the EHB model, shown in **Figure 4** and in **Figure 5**.

The Extended Herringbone-like (EHB) structure explained:

In contrast to the well-known planar bricklayer structure [5], the novel EHB structure was designed by using a herringbone-like structure where the unit cells are rotated out of plane, which then is again wrapped around a cylindrical surface. The EHB structure is constructed by starting out from a planar (*x*-*y* plane) bricklayer structure, characterized by lattice vectors $\mathbf{a}_1$ and $\mathbf{a}_2$, where each C8S3 molecule is represented by a brick with length *a* and width *d*. The transition dipole moment of the C8S3 molecule has magnitude μ and is oriented in the direction of the long axis.

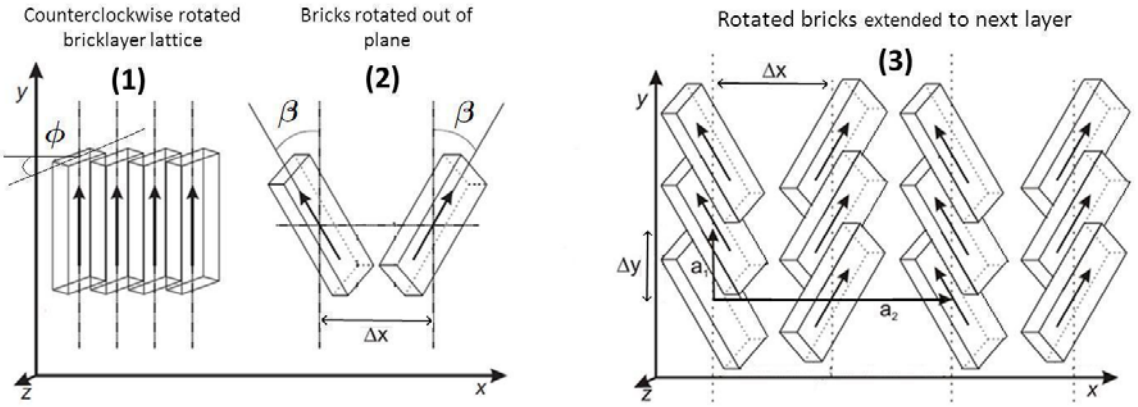

Figure S4: Schematic representation of the newly designed structure for an isolated cylindrical aggregate: the Extended Herringbone-like (EHB) structure. (1) and **(2)** show the rotations that are applied to the molecules that are initially in a planar bricklayer geometry. **(3)** shows the final relative orientation for four rows of three molecules. The molecular structure of the tubular aggregate is obtained by rolling the planar geometry in **(3)** onto a cylindrical surface of appropriate radius.

The EHB geometry is now generated by allowing for two rotations of the C8S3 molecules. First, all C8S3 molecules are rotated over an angle ϕ around the *y*-axis (**Figure S4(1)**). For future reference, we refer to this rotation by its complementary angle δ (i.e., $\delta=\pi/2-\phi$). Subsequently, all molecules are rotated around the *x*-axis by, alternatingly, an angle β and an angle $-\beta$ (**Figure S4(2)**). Note that this latter step generates a lattice with two molecules per unit cell (**Figure S4(2)**), as is required in order to produce four peaks in the absorption spectrum. Clearly, after these rotations the C8S3 molecules and thus also their transition dipole moments are tilted out of the original planar lattice (**Figure S4(3)**). It follows that the distance Δx between adjacent rows in the *x*-direction is not directly determined by the dimensions of the C8S3 molecule, but rather by the interactions between the parallel oriented phenyl rings of the C8S3 molecules (see **Section 5**). This high degree of π-stacking plays a major role in determining the details of the molecular arrangement in this system. Finally, the distance between molecules in the *y*-direction Δy may be obtained from optimal packing conditions, i.e., we assume that the spacing between them is minimal (see **Section 5**).

To model the molecular structure of each cylindrical wall, the planar geometry in **Figure S4(3)** is rolled onto a cylindrical surface by defining a chiral vector that connects two lattice points, such that these points coincide after the rolling [3]. The chiral vector is defined by the wrapping angle θ it makes with the x-axis, and by its length which equals the circumference of the cylinder. After rolling the above structure onto a cylindrical surface, all molecular positions and orientations can be defined in the commonly used stack-of-rings representation [3], albeit with two molecules per unit cell. We use the notation $\vec{n} = (n_1, n_2)$ for the unit cell located at the n_1-th ring (n_1=1,2,..., N_1) and the n_2-th helix (n_2=1,2,... N_2) and the label j=1,2 for the two molecules within the unit cell. Defining the Cartesian unit vectors in the cylinder frame by respectively e_x, e_y and e_z (where e_z is the direction of the cylinder axis), the position and orientation of molecule j in unit cell $\vec{n}$ are given by

$$\vec{r}_{n,j} = R\cos\left(n_1\gamma + n_2\phi_2 + \delta_{j,2}\Delta\phi\right)\hat{e}_x + R\sin\left(n_1\gamma + n_2\phi_2 + \delta_{j,2}\Delta\phi\right)\hat{e}_y + \left(n_1 h + \delta_{j,2}\Delta z\right)\hat{e}_z \quad \textbf{(S1)}$$

and

$$\begin{aligned}\vec{\mu}_{n,j} = &\left[\mu_{z,j}\cos\left(n_1\gamma + n_2\phi_2 + \delta_{j,2}\Delta\phi\right) - \left(\mu_{x,j}\cos\theta + \mu_{y,j}\sin\theta\right)\sin\left(n_1\gamma + n_2\phi_2 + \delta_{j,2}\Delta\phi\right)\right]\hat{e}_x + \\ &\left[\mu_{z,j}\sin\left(n_1\gamma + n_2\phi_2 + \delta_{j,2}\Delta\phi\right) + \left(\mu_{x,j}\cos\theta + \mu_{y,j}\sin\theta\right)\cos\left(n_1\gamma + n_2\phi_2 + \delta_{j,2}\Delta\phi\right)\right]\hat{e}_y + \\ &\left(-\mu_{x,j}\sin\theta + \mu_{y,j}\cos\theta\right)\hat{e}_z.\end{aligned} \quad \textbf{(S2)}$$

Here, we have defined $\phi_2 = 2\pi / N_2$, the quantity $\delta_{j,2}$ is the Kronecker delta signifying that the origin of the unit cell is chosen to coincide with molecule $j = 1$, and the factors $\mu_{x,j}$, $\mu_{y,j}$ and $\mu_{z,j}$ are the three Cartesian components of the transition dipole moment of molecule j in the original planar coordinate system. Finally, the two quantities $\Delta\phi$ and Δz define the relative position of the two molecules in the unit cell and are the components in the azimuthal direction and the axis direction, respectively. The parameter choices and the fitting procedure for the remaining quantities are detailed in **Section 5**.

The optical electronic excitations are described by a Frenkel exciton Hamiltonian, in which the molecules are considered two-level systems. Accounting for molecular transition energies as well as intermolecular resonance transfer interactions (that give rise to delocalized (extended) excitations), the Frenkel Hamiltonian for a single cylindrical aggregate reads,

$$H = E_0 \sum_{\vec{n},j} \left|\vec{n},j\right\rangle\left\langle\vec{n},j\right| + \sum_{\vec{n},\vec{m},i,j} J(\vec{n},i;\vec{m},j)\left|\vec{n},i\right\rangle\left\langle\vec{m},j\right|. \qquad \textbf{(S1)}$$

Here $\left|\vec{n},j\right\rangle$ denotes the state where only the j^{th} molecule (j=1,2) in the unit cell $\vec{n}$ is in its excited state, whereas all other molecules are in their ground state. The excitation energies E_0 are assumed identical for all molecules, thus neglecting the effects of electronic disorder. The resonance interactions $J(\vec{n},i;\vec{m},j)$ between pairs of molecules are obtained using extended transition dipoles [5,6]. The exciton eigenstates and energies are then determined by numerical diagonalization of the above Hamiltonian, which allows for calculation of the linear optical absorption spectra using standard methods [3].

5. Parameters and fitting procedure

The geometrical parameters involved in **Eqs. S1** and **S2** (**Section 4**) are determined experimentally, taken from the literature, or fitted. The parameters a and d specify the dimensions of the C8S3 molecule and are thus related to its size are taken from [3, 5, 6] as a=2.0 nm and d=0.4 nm. The typical radius of the outer wall nanotube was determined experimentally from line scans taken from Cryo-TEM images, which yields a radius of R_{OW}=6.5±0.5 nm. To determine the radius of the inner wall cylinder, the double-walled nanotube was first filled with silver after which line scans of the Cryo-TEM images were taken to determine the radius of the silver nanowire, which yields a diameter of D_{IW}=6.4±0.5 nm [1]. However, in this way the measured diameter does not reflect the center positions of the molecules, but of the sulfite groups. To compensate for this, we take a slightly higher value for the inner wall radius, R_{IW}=3.5±1.0 nm. The geometrical parameter Δx (**Figure S4**) is the distance between molecules in the unit cell in the x-direction. This distance is mainly determined by the interaction between the phenyl rings of the C8S3 molecules, which are approximately oriented parallel to each other, and is thus mostly the result of π-stacking. The value is taken from [7] and is in our simulations given by Δx=0.55 nm. Finally, the geometrical parameter Δy (**Figure S4**) denotes the distance between molecules in the y-direction. This parameter can be obtained by assuming that the molecules stacked on top of each other are optimally packed. This gives the relation $\Delta y = d/\sin(\beta)$, where the rotation angle β is restricted to values β>11.3°.

The relevant energetic parameters are the monomer transition energy E_0, and the extended dipole charges Q and distances L, which together should reproduce the monomer transition dipole moment. The values of all these parameters have previously been reported in [5] and have the explicit values $E_0 = 18868$ cm^{-1}, Q=0.34e and L=0.7 nm. These values correspond to a monomer transition wavelength of λ=530 nm and a transition dipole of magnitude μ=11.4 D. Generally, upon aggregation there might be energetic shifts present for a number of reasons, such as interactions being different

depending on whether a molecule is in the ground state or in the excited state, solvent shifts, disorder-induced shifts and shifts due to coupling to vibrational modes [8]. Therefore, when determining the best fit to experiment, we focus on the energy (frequency) separations between the various peaks in the absorption spectra, and allow for an additional overall energy shift to align the absolute position of the numerical spectra with experiment. The shift depends on the exact fit parameters, and has a magnitude of 417 cm^{-1} for the parameters obtained below, which is of a comparable magnitude to what has been used in previous studies in different cylindrical aggregates [5].

This leaves us in principle with three geometrical parameters that are determined by fitting, being two geometrical rotation angles (β and δ) and the wrapping angle θ that determines how the two-dimensional lattice is rolled onto the cylindrical surface. Note that we require that the calculated absorption spectra reproduce the (relative) energies, polarizations and relative oscillator strengths of four peaks; three fit parameters is thus not an excessively large number.

For the inner-wall cylinder, optimal agreement with the experimentally obtained spectrum is found for R_{IW}=3.55 nm, β_{IW}=23.6°, δ_{IW}=25.6° and θ_{IW}=53.7°, as shown in **Figure 5a**. In these simulations, the number of molecules in the inner wall is taken as N_{IW}=7992, corresponding to a tube length of L_{IW}=197 nm.

The outer-wall cylinder is also modeled by an EHB structure, where the parameters are fitted by requiring an optimal agreement between the calculations of the absorption spectrum of the double wall system and the experimental absorption spectrum. The outer wall parameters that result are R_{OW}=6.48 nm, β_{OW}=23.1°, δ_{OW}=28.0° and θ_{OW}=53.5°, showing that the thus obtained geometries of inner wall and outer wall are very similar. Note that these parameters imply a minimum distance between inner and outer wall chromophores of 2.93 nm; typically, the inner and outer wall lattices are incommensurate which will lead to larger distances for most molecules. We again use a total tube length of L=197 nm, which corresponds to N_{OW}=14260 molecules in the outer wall.

To test the range of validity of the set of optimal geometrical angles for the inner wall, we first varied all three parameters separately; keeping the other two fixed at their optimal value and compared the resulting spectra with the experimental data. We found that the rotation angles could be varied up to β_{IW}=23.6±0.1° and δ_{IW}=25.6±0.5°, while still retaining good agreement with the experimentally observed isolated inner wall spectrum. For the rolling angle we found an error margin of roughly θ_{IW}=53.7±3°. Here we note that due to the discrete nature of the plane that is wrapped around the cylinder, this angle can only take on certain discrete values, in contrast to the continuous nature of the rotation angles. Moreover, adjusting the rolling angle is accompanied by variations in the radius of the inner wall cylinder, R_{IW}=3.55±0.3 nm, which remains well within the limits set by the Cryo-TEM observations.

As a next step, we varied all three geometrical parameters of the inner-wall cylinder simultaneously around their optimal values to specify the region of the three-dimensional parameter space where unique sets of geometrical angles can be found that give good agreement with the experimental absorption spectra. We observed that within the space limited by roughly one degree variation for the rotation angle β_{IW} and several degrees of variation for the other two angles, multiple sets of geometrical parameters could be found that correctly reproduce the relative energy positions and polarization directions, and yielded reasonable intensities for the four transition bands. From these possible structures, the optimal geometry was determined as the structure which could give the correct intensities of the absorption peaks, while maintaining the overall energy shift minimal.

We have also performed simulations including static disorder in the transition energies of the individual molecules. No significant improvement was found in the thus obtained fit of the absorption spectrum and no significant change in the structural parameters was obtained from the best fit. The disorder strength (standard deviation of the Gaussian disorder distribution) was found to be at most 250 cm^{-1}.

6. References

[1] Eisele, D. M. et al. Photoinitiated growth of sub-7nm silver nanowires within a chemically active organic nanotubular template. *J. Am. Chem. Soc.* **132,** 2104-2105 (2010).

[2] Brand, L. & Johnson, M. L. *Methods In Enzymology: Numerical Computer Methods, Vol 210* (San Diego: Academic Press, 1992).

[3] Didraga, C., Klugkist, J. A. & Knoester, J. Optical properties of helical cylindrical molecular aggregates: the homogeneous limit. *J. Phys. Chem. B* **106**, 11474–11486 (2002).

[4] von Berlepsch, H., Kirstein, S., Hania, R., Pugzlys A. & Böttcher, C. Modification of the nanoscale structure of the J-aggregate of a sulfonate-substituted amphiphilic carbocyanine dye through incorporation of surface-active additives. *J. Phys. Chem. B* **111**, 1701–1711 (2007).

[5] Didraga, C. et al. Structure, spectroscopy, and microscopic model of tubular carbocyanine dye aggregates. *J. Phys. Chem. B* **108,** 14976-14985 (2004).

[6] Czikkely, V., Försterling, H. D. & Kuhn, H. Light absorption and structure of aggregates of dye molecules. *Chem. Phys. Lett.* **6,** 11-14 (1970). *Ibid.* Extended dipole model for aggregates of dye molecules. *Chem. Phys. Lett.* **6,** 207-210 (1970).

[7] Jorgensen, W. L. & Severance, D. L. Aromatic-aromatic interactions: free energy profiles for the benzene dimer in water, chloroform, and liquid benzene. *J. Am. Chem. Soc.* **112,** 4768-4774 (1990).

[8] Davydov, A. S. *Theory of Molecular Excitons* (Plenum: New York, 1971).